Journal of Nuclear Medicine, published on February 3, 2022 as doi:10.2967/jnumed.121.263255

Assessing reactive astrogliosis with ^{18}F-SMBT-1 across the Alzheimer's disease spectrum

Victor L Villemagne,[1,2] Ryuichi Harada,[3,4] Vincent Doré,[1,5] Shozo Furumoto,[6] Rachel Mulligan,[1] Yukitsuka Kudo,[4] Samantha Burnham,[5] Natasha Krishnadas,[1] Pierrick Bourgeat,[7] Ying Xia,[7] Simon Laws,[8] Svetlana Bozinovski,[1] Kun Huang,[1] Milos D. Ikonomovic,[2,9,10] Jürgen Fripp,[7] Kazuhiko Yanai,[3] Nobuyuki Okamura[11] and Christopher C Rowe.[1,12,13]

1. *Department of Molecular Imaging & Therapy, Austin Health, Melbourne, Australia*
2. *Department of Psychiatry, University of Pittsburgh, Pittsburgh, PA, USA.*
3. *Department of Pharmacology, Tohoku University School of Medicine, Sendai, Japan*
4. *Institute of Development of Aging and Cancer, Tohoku University, Sendai, Japan*
5. *CSIRO Health and Biosecurity Flagship: The Australian e-Health Research Centre, Melbourne, Australia*
6. *Cyclotron and Radioisotope Center, Tohoku University, Sendai, Japan*
7. *CSIRO The Australian e-Health Research Centre, Brisbane, Australia*
8. *School of Medical and Health Sciences, Edith Cowan University, Perth, Australia.*
9. *Department of Neurology, University of Pittsburgh, Pittsburgh, PA, USA*
10. *Geriatric Research Education and Clinical Center, VA Pittsburgh Healthcare System, Pittsburgh, PA, USA.*
11. *Division of Pharmacology, Faculty of Medicine, Tohoku Medical and Pharmaceutical University, Sendai, Japan*
12. *The Florey Institute of Neurosciences and Mental Health, The University of Melbourne, Melbourne, Australia*
13. *The Australian Dementia Network*

Corresponding author: Victor L Villemagne
Address: Department of Psychiatry, University of Pittsburgh School of Medicine, 3811 O'Hara St. Pittsburgh PA, 15213, USA.
Tel: +1 412-246-6010
Email: victor.villemagne@pitt.edu

Key Words: Reactive astrogliosis, MAO-B, Alzheimer's disease, amyloid, tau, brain imaging

Running Title: *Reactive astrogliosis in AD.*

Disclosure*: Yukitsuka Kudo and Nobuyuki Okamura own stock in Clino Ltd licensing SMBT-1. Ryuichi Harada, Shozo Furumoto, Yukitsuka Kudo, and Nobuyuki Okamura have a patent pending for the technology described in this article. The rest of the authors report no conflict of financial interest in relation to this work.*

ABSTRACT

Background: Neuroinflammatory reaction in Alzheimer's disease (AD) brains involves reactive astrocytes which overexpress monoamine oxidase-B (MAO-B). ^{18}F-SMBT-1 is a novel F-18 PET tracer highly selective for MAO-B. We characterized the clinical performance of ^{18}F-SMBT-1 PET across the Alzheimer's disease (AD) continuum as a potential surrogate marker of reactive astrogliosis

Methods: We assessed ^{18}F-SMBT-1 PET regional binding in 77 volunteers (76±5.5 y.o.; 41F/36M) across the AD continuum: 57 cognitively unimpaired controls (CN, 44 Aβ- & 13 Aβ+), 12 mild cognitively impaired (MCI, 9 Aβ- & 3 Aβ+), and 8 AD dementia patients (6 Aβ+ and 2 Aβ-). All participants also underwent Aβ and tau PET imaging, 3T MRI and neuropsychological evaluation. Tau imaging results were expressed in standard uptake value ratios (SUVR) using the cerebellar cortex as reference region, while Aβ burden was expressed in Centiloids. ^{18}F-SMBT-1 outcomes were expressed as SUVR using the subcortical white matter as reference region.

Results: ^{18}F-SMBT-1 yielded high contrast images at steady state (60-80 min after injection). When compared to Aβ-CN, there were no significant differences in ^{18}F-SMBT-1 binding in the Aβ-MCI group. Conversely, ^{18}F-SMBT-1 binding was significantly higher in several cortical regions in the Aβ+AD group, but also was significantly lower in mesial temporal and basal ganglia. Most importantly, ^{18}F-SMBT-1 binding was significantly higher in the same regions in Aβ+CN when compared to Aβ-CN. When all clinical groups were considered together, ^{18}F-SMBT-1 was highly correlated with Aβ burden, and much less with tau burden. While in most cortical regions ^{18}F-SMBT-1 was not correlated with brain volumetrics, regions known for high MAO-B concentrations presented a direct association with hippocampal and grey matter volumes, while the occipital lobe was directly associated with white matter hyperintensities. ^{18}F-SMBT-1 binding was inversely correlated with MMSE and AIBL PACC in some neocortical regions such as the frontal cortex, lateral temporal and supramarginal gyrus.

Conclusions: Cross-sectional human PET studies with ^{18}F-SMBT-1, showed that Aβ+AD, but most importantly, Aβ+CN have significantly higher regional ^{18}F-SMBT-1 binding than Aβ- CN. Moreover, in several regions in the brain, ^{18}F-SMBT-1 retention was highly associated with Aβ load. These findings suggest that increased ^{18}F-SMBT-1 binding is detectable at the preclinical stages of Aβ accumulation, providing strong support for its use as surrogate marker of astrogliosis in the AD continuum.

INTRODUCTION

The neuropathological hallmarks of Alzheimer's disease (AD), neurofibrillary tangles (NFT) of tau protein and amyloid-β (Aβ) plaques, are accompanied by reactive gliosis, cellular degeneration, and diffuse synaptic and neuronal loss. (*1*) Astrocytes are the most abundant glial cells in the brain and are involved in several functions critical for the normal functioning and preservation of brain homeostasis (*2,3*) Loss of these regulatory and compensatory mechanisms in astrogliosis likely translates in an increased vascular-related vulnerability state, (*4*) affecting the brain's ability to compensate for the accumulating Aβ and tau pathology burden and impaired cerebrovascular function in AD. The complex spectrum of toxic and protective pathways (*5,6*) of reactive astrogliosis, play a crucial role in the pathophysiology of AD (*7-9*) and other neurodegenerative conditions. (*10-16*) Reactive astrogliosis and microgliosis have been observed around both dense-core Aβ plaques and neurofibrillary tangles, and they are believed to contribute greatly to neurodegeneration throughout the course of AD (*9,17*). In contrast to microgliosis (*18*) reactive astrogliosis occurs early in the disease, (*19*) and is a particularly attractive target for understanding its contribution to the development of AD dementia and, as such, a potential therapeutic target for AD (*20*).

Reactive astrocytes overexpress monoamine oxidase B (MAO-B), (*21*) and molecular neuroimaging studies have employed MAO-B tracers such as ^{11}C-L-deprenyl-D2 (^{11}C-DED) and ^{11}C-SL25.1188 (*22,23*) as surrogate markers of astrogliosis. (*15,19,24-26*) Some of these studies have shown that reactive astrogliosis is observed at the prodromal stages in both sporadic and familial AD. (*19,24*) ^{11}C-BU99008 a tracer for the imidazoline 2 binding sites —with some partial binding to MAO-B (*27*)— has also been proposed as a surrogate marker of astrogliosis. (*28,29*) Unfortunately, these tracers are labeled with 20-min half-life C-11 preventing widespread clinical or research applications.

A novel F-18 MAO-B tracer [^{18}F]*(S)*-(2-methylpyrid-5-yl)-6-[(3-fluoro-2-hydroxy)propoxy]quinoline (^{18}F-SMBT-1), with high in vitro binding affinity (K_D=3.5 nM) and selectivity to MAO-B, has been recently developed (*30*). Comparison of in vitro ^{18}F-SMBT-1 binding against MAO-B activity showed SMBT-1 binding to be highly correlated with the regional activity of MAO-B in AD brain tissue homogenates (*30*). Autoradiography analysis showed significantly higher specific binding in the frontal cortex tissue section from an AD patient compared to control (*30*), which was completely displaced by the selective MAO-B inhibitor lazabemide (*30*).

In first-in-human studies, (*31*) ^{18}F-SMBT-1 showed robust entry into the brain and reversible binding kinetics, where quantitative and semiquantitative measures of ^{18}F-SMBT-1 binding were highly associated. More than 85% of ^{18}F-SMBT-1 signal was blocked by selegiline across the brain indicating high selectivity for MAO-B and low non-specific binding. ^{18}F-SMBT-1 regional binding followed the known regional brain distribution of MAO-B (R^2=0.84), while also capturing the known MAO-B increases with age. (R^2>0.94), suggesting ^{18}F-SMBT-1 can potentially be used as a surrogate marker of reactive astrogliosis in AD.

The aim of this study was to characterize ^{18}F-SMBT-1 binding across the AD continuum, assessing its relation to Aβ and tau pathology burden, as well as brain volumetrics, white matter hyperintensities (WMH) and cognitive performance.

MATERIALS AND METHODS

Participants

A total of 77 non-smoking elderly participants (76±5.5 y.o. age range 58-89; 40F/35M) were included in the study: 57 cognitively unimpaired controls (CN) 12 subjects meeting criteria for mild cognitive impairment (MCI) (*32*), and 8 subjects meeting NINDS-ADRDA *and* NIAA-AA criteria for AD (*33*). Subjects with AD and MCI were recruited from Memory Disorders Clinics. Cognitively normal subjects were recruited by advertisement in the community. Some participants (46 CN, 6 MCI and 4 AD) were included in a previous study. (*31*)

All participants were screened for unstable medical and/or psychiatric disease and concomitant medication. Participants with known use MAO-B inhibitors or with a diagnosis of a psychiatric disorder were excluded from the study. For participants with a recognized memory impairment, this information was collected from a next of kin or caregiver. The study protocol was approved by the Austin Health Human Research Ethics Committee, and all participants gave written informed consent.

A detailed neuropsychological evaluation is provided in Supplementary materials

Image Acquisition

PET

All SMBT-1 PET scans were acquired on the Philips TF64 PET/CT. Aβ and tau PET scans were acquired on one of two scanners, a Philips TF64 PET/CT or a Siemens Biograph mCT. A low dose CT was obtained for attenuation correction.

^{18}F-SMBT-1 imaging

All 77 participants underwent ^{18}F-SMBT-1 PET. As previously reported (*31*), 10 non-demented participants (4 CN and 6 MCI) underwent a 90 min dynamic scanning after intravenous bolus injection of 185 MBq (±10%) of ^{18}F-SMBT-1. The remaining 67 participants received an intravenous bolus injection of 185 MBq (±10%) of ^{18}F-SMBT-1 and a 20-minute emission scan (4 x 5 min) starting at 60 minutes post injection.

^{18}F-SMBT-1 was synthesized in-house in the Department of Molecular Imaging & Therapy, Austin Health, using as previously described (*31*) ^{18}F-SMBT-1 yielded a greater than 95% radiochemical purity after HPLC purification, with an average decay-corrected radiochemical yield of 40% and the molar activity at the end of ^{18}F-SMBT-1 synthesis >400 GBq/μmol.

Aβ imaging

All 77 participants underwent Aβ PET imaging with either ^{18}F-Flutemetamol (FLUTE, n=3), Florbetapir (FBP, n=2) or ^{18}F-NAV4694 (NAV, n=72) to ascertain Aβ status. NAV and FBP were synthesized in-house in the Department of Molecular Imaging & Therapy, Austin Health, as previously described. (*34,35*) FLUTE was manufactured by Cyclotek Pty Ltd, (www.cyclotek.com). The NAV and FBP PET scan acquisitions consisted of a 20 minute (4 x 5 min) dynamic scans acquired at 50 minutes after an intravenous bolus injection of 200 MBq (±10%) of NAV or FBP. Similarly, the participants who received FLUTE PET scans also underwent a 20-minute (4 x 5 min) acquisition starting at 90 minutes after injection of 185 MBq (±10%) of FLUTE. All Aβ imaging results were expressed in Centiloids (CL). (*34-38*). In a subset of participants (n=31) that had available longitudinal Aβ imaging data, rates of Aβ accumulation –expressed as CL/yr- were generated from the linear regression of the data as previously described. (*39*)

Tau imaging

Seventy-four participants underwent tau imaging with either ^{18}F-MK6240 (n=70) or ^{18}F-PI2620 (n=2). Both tau imaging tracers were synthesized in-house in the Department of Molecular Imaging &

Therapy, Austin Health, as previously reported. (*40,41*) The ^{18}F-MK6240 PET scan acquisition consisted of a 20 minute (4 x 5 min) dynamic scans acquired at 90 minutes after an intravenous bolus injection of 185 MBq (±10%) of ^{18}F-MK6240. The ^{18}F-PI2620 PET scan acquisition consisted of a 20 minute (4 x 5 min) dynamic scans acquired at 80 minutes after an intravenous bolus injection of 200 MBq (±10%) of ^{18}F-PI2620. All tau imaging results were expressed as standard uptake value ratios (SUVR) using the cerebellar cortex as reference region. A meta-temporal region, comprising the entorhinal cortex, amygdala, hippocampus, parahippocampal gyrus, fusiform gyrus, inferior and middle temporal gyri, – adapted from (*42*)– was used to determine tau status (T) and for the correlational analysis.

MRI

Seventy-three participants underwent a structural magnetic resonance imaging (MRI) on a Siemens 3-T TIM Trio scanner (Siemens Medical Solutions) to obtain high-resolution T1-weighted anatomical magnetization prepared rapid gradient echo (MPRAGE) and fluid-attenuated inversion recovery (FLAIR) sequences.

Image Analysis

Aβ and tau PET scans were spatially normalized using CapAIBL. (*38*) The standard Centiloid (CL) method was applied to determine Aβ burden. (*36*) A threshold of 20 CL was used to categorize participants as high Aβ (Aβ+) or low Aβ (Aβ-) (*43*). Thresholds of 1.19 SUVR for ^{18}F-MK6240 and 1.20 SUVR for ^{18}F-PI2620 in the meta-temporal composite region (*42*) were used to categorize participants as high tau (T+) or low tau (T-). As previously described (*31*), assessment of the stability of potential reference regions for ^{18}F-SMBT-1 across age and across groups showed no associations with age, but the cerebellar cortex was significantly higher in Aβ+ CN when compared to Aβ- CN, precluding its use as reference region. Therefore, ^{18}F-SMBT-1 regional standard uptake values (SUV) at 60-80 min post injection were normalized using the subcortical white matter (SWM) as reference region to generate semiquantitative tissue ratios/SUVR. ^{18}F-SMBT-1 PET images were spatially normalized using CapAIBL, and no correction for partial volume effects (PVE) was applied.

The T1 weighted MPRAGE images for all participants were first segmented into grey matter (GM), white matter (WM) and cerebrospinal fluid using an implementation of expectation maximization algorithm (*44*), and subsequently used to measure hippocampal (HV), GM, WM and ventricular volumes. The hippocampus ROI was extracted using a multi-atlas approach based on the Harmonized Hippocampus Protocol (*45*). Cortical volumes were normalized by Total Intracranial Volume (TIV). The WMH volume was quantified from FLAIR images using the HyperIntensity Segmentation Tool (*46*).

Statistical analyses

All statistical analyses were performed with JMP Pro 16.0 for Macintosh (JMP® Pro Version 16, SAS Institute Inc., Cary, NC, 1989-2021). Data are presented as mean ± standard deviation (SD) unless otherwise stated. Statistical evaluations between groups were performed using Tukey honest significance test followed by a Dunnett's test against Aβ- CN. Effect size was measured with Cohen's d. Correlations were assessed by Spearman and Pearson correlation coefficients. Vertex-wise correlations between ^{18}F-SMBT-1 and Aβ and tau imaging were performed with CapAIBL. The two participants that underwent tau imaging with ^{18}F-PI2620 were excluded from the correlational analysis. Group comparisons ^{18}F-SMBT-1 and correlation between SMBT-1 and Aβ or tau burdens were adjusted for age and sex. Correlations between ^{18}F-SMBT-1 and brain volumes were adjusted for age, sex, and also to Aβ and tau burdens. Correlations between ^{18}F-SMBT-1 and cognitive parameters were also adjusted to age, sex, hippocampal volume, and Aβ and tau burdens. Significance was set at $p<0.05$, uncorrected for multiple comparisons.

RESULTS

Table 1 shows the demographics of the clinical groups. There were no significant differences in age, between the clinical groups. The MCI group had twice the proportion of males in contrast to the CN and AD group that had more females than males. The MCI and AD groups had significantly less years of education. As expected, the MCI and AD groups presented with significant worse cognitive performance when compared to CN. (Table 1) The AD group had significantly more atrophic hippocampi and cortical GM, more extensive WMH, higher Aβ and tau burdens, as well as a higher prevalence of APOE4. (Table 1). Demographics of participants classified by Aβ status is provided in Supplementary Table 1.

^{18}F-SMBT-1 yielded high contrast SUV images at steady state (60-80 min after injection). Figure 1 shows representative ^{18}F-SMBT-1 images from Aβ- CN, Aβ+ CN, Aβ- MCI, Aβ+ MCI and Aβ+ AD subjects. When comparing the clinical groups against the CN group, ^{18}F-SMBT-1 binding was significantly higher in several regions in the AD (including the two Aβ- "AD" subjects) group, namely posterior cingulate, supramarginal gyrus and lateral occipital, but also was significantly lower in globus pallidus, hippocampus and parahippocampal gyrus.

Then the clinical groups were classified based on their Aβ status. Of the 57 CN, 44 were Aβ- and 13 Aβ+. Of the 12 MCI, 9 were Aβ- and 3 Aβ+, while of the 8 probable AD patients 6 were Aβ+ and 2 Aβ-. When compared to Aβ- CN, there were no significant differences in ^{18}F-SMBT-1 binding in either the Aβ- MCI and Aβ- AD group. (Supplementary Table 2) In contrast, when compared to Aβ- CN, ^{18}F-SMBT-

1 binding was significantly higher in several cortical regions in the Aβ+ AD group, (Figure 2) namely posterior cingulate, supramarginal gyrus, lateral occipital, gyrus angularis and primary visual cortex but also was significantly lower in globus pallidus and hippocampus, with Cohen's effect sizes (*d*) ranging from 2.65 and 2.36 in lateral occipital and supramarginal gyrus, respectively, to -1.66 and -1.88 in hippocampus and globus pallidus, respectively. (Supplementary Table 2) Several regions were also significantly higher in Aβ+ CN when compared to Aβ- CN. (Figure 2) In addition to posterior cingulate, supramarginal gyrus, lateral occipital –the same regions with high binding in Aβ+ AD– ^{18}F-SMBT-1 binding was also significantly higher in orbitofrontal, lateral and inferior temporal gyri. ^{18}F-SMBT-1 binding was also significantly lower in the globus pallidus. (Supplementary Table 2) The effect sizes (*d*) ranged from 1.21 and 1.00 in supramarginal gyrus and lateral temporal, respectively, to -1.29 in globus pallidus. (Supplementary Table 2) Similar regions, like the supramarginal gyrus, showed higher ^{18}F-SMBT-1 binding in the Aβ+ MCI group, but none reached significance. (Figure 2)

When all clinical groups were considered together, ^{18}F-SMBT-1 PET was highly correlated with Aβ burden and much less with tau burden. (Table 2) Figure 3A shows that this close regional relationship between Aβ deposition and astrogliosis is only present in some regions of the brain like the supramarginal gyrus, posterior cingulate, lateral occipital and inferior and middle temporal gyri while it is much lower in other regions also characterized by high Aβ deposition such as the frontal cortex, and relatively absent in superior temporal gyrus. When further exploring the relationship between ^{18}F-SMBT-1 and Aβ we observed that a non-linear fit seems to better describe the relationship between ^{18}F-SMBT-1 and Aβ in, for example, the supramarginal gyrus where the ^{18}F-SMBT-1 signal seems to be increasing before Aβ becomes abnormal. (Supplementary Figure 1) This relationship was not affected after adjusting for age, WMH and hippocampal volume. There were no correlations between ^{18}F-SMBT-1 and Aβ in brain regions with high density of MAO-B such as the anterior cingulate gyrus and the mesial temporal lobe (MTL). Further, in the basal ganglia, the region with the highest density of MAO-B in the brain, ^{18}F-SMBT-1 was inversely correlated with Aβ. (Table 2) A similar picture was observed when ^{18}F-SMBT-1 was correlated with tau in the meta-temporal region, although the associations were less extensive (Figure 3B) and reached lower significance levels than with Aβ. (Table 2) When examining the relationship between ^{18}F-SMBT-1 and Aβ accumulation in a subset of participants (n=31) that had available longitudinal Aβ imaging data, a significant association was observed in the temporal lobe (lateral and inferior temporal). (Table 2) Trend levels ($p<0.09$) were also observed in the parahippocampus, temporooccipital and supramarginal gyrus regions. (Table 2)

When all clinical groups were considered together, Aβ and tau burdens were highly associated with HV and GM volumes. (Supplementary Table 3) Overall, sex was the major contributor to the variation in GM volumes, while age was the major contributor to the variation in WMH. A few associations survived after co-variate adjustment. ^{18}F-SMBT-1 binding in the supramarginal gyrus and lateral occipital were inversely associated with GM (r=-0.28, p=0.017) and HV (r=-0.28, p=0.016), respectively, (Supplementary Table 3) Conversely, ^{18}F-SMBT-1 binding in the hippocampus was significantly associated with HV (r=0.34, p=0.003), cortical GM (r=0.34, p=0.004) and WM volumes (r=0.23, p=0.048), but theirs was a direct relationship, in other words, the lower the ^{18}F-SMBT-1 binding the lower the respective volumes. (Supplementary Table 2) Similar findings were observed in the caudate, pallidus, thalamus and pons where ^{18}F-SMBT-1 binding was also directly associated with GM volumes. (Supplementary Table 3) In contrast to the findings in the MTL, there was no atrophy detected in these regions. ^{18}F-SMBT-1 binding in the occipital lobe was significantly associated with WMH. (Supplementary Table 3)

When all groups were considered together, and after adjusting for age, sex, Aβ, tau and HV, ^{18}F-SMBT-1 binding was correlated with MMSE and AIBL PACC in some neocortical regions such as the frontal cortex, lateral temporal, supramarginal gyrus and angular gyrus, contributing 24-35% of the variance of MMSE, and 18-28% of the variance of AIBL PACC. (Table 3) Overall, all cognitive domains were driven by tau, with HV contributing to CDR SoB, Non-memory and AIBL PACC, and sex contributing to Episodic Memory and AIBL PACC.

DISCUSSION

To the best of our knowledge, ^{18}F-SMBT-1 represents the first available F-18 MAO-B radiotracer to be used in a clinical study to assess reactive astrogliosis. In the present clinical study we evaluated the performance of ^{18}F-SMBT-1 PET across the AD spectrum.

When comparing clinical groups, the AD group presented with both significantly higher (posterior cingulate, supramarginal gyrus) and lower (hippocampus, globus pallidus) SMBT-1 binding than observed in cognitively normal elderly controls. This difference was better defined when the clinical groups where separated based on having high or low Aβ PET burden. It became clear that in regions like posterior cingulate, supramarginal gyrus and lateral occipital, Aβ+ CN and Aβ+ AD became better separated from Aβ- CN, but also that globus pallidus and hippocampus remained significantly lower. Interestingly, the same regions tended to be higher in Aβ+ MCI but it was a group with only 3 participants

and none of the regions achieved significance. Most importantly, Aβ+ CN had significantly higher ^{18}F-SMBT-1 binding compared to Aβ- CN in the same regions that were significantly higher in the AD group (posterior cingulate, supramarginal gyrus, lateral occipital), but it was also significantly higher in orbitofrontal, lateral and inferior temporal gyri. These findings match recent reports from fluid biomarker studies that found that plasma levels of glial fibrillary acidic protein (GFAP), an astrocytic marker, is higher in Aβ+ CN when compared to Aβ- CN, (*47*) as well as predicting future conversion to AD in MCI subjects. (*48*)

As in the AD group, when compared to Aβ- CN, ^{18}F-SMBT-1 binding in Aβ+ CN was significantly lower in the globus pallidus. The first thing to consider when looking at the mesial temporal structures is that the PET results are not corrected for PVE, and as expected, the hippocampi in the Aβ+ AD group were significantly more atrophic than in the Aβ- CN group (5.94±0.5 vs. 4.50±0.5, $p<0.0001$), and while this is likely the best explanation for lower ^{18}F-SMBT-1 binding in a region that otherwise has a high density of MAO-B. On the other hand, PVE are not likely to explain the lower ^{18}F-SMBT-1 binding in the region with the highest density of MAO-B in the brain. While only the globus pallidus reached significance, all basal ganglia regions showed lower ^{18}F-SMBT-1 binding, (Figure 2). An alternative explanation might be that, as in vitro studies using autoradiography and ^{11}C-DED showed, MAO-B presented an inverse correlation with Braak & Braak stages in AD brains (*49*) suggesting that as the neurodegeneration progresses the expression of MAO-B is decreasing, most noticeably in those areas with high density of MAO-B like the MTL and basal ganglia while also reflecting the regional loss of astrocytes similar to what is observed in neurons (*50*) associated with progressive Aβ deposition.

When considering that the brain regions with significantly higher SMBT-1 binding in Aβ+ CN and Aβ+ AD, such as the supramarginal gyrus (identified as “temporoparietal junction” in 2012 (*51*) and recently rebranded as the “banks of the superior temporal sulcus” (*52*)), along the orbitofrontal and the posterior cingulate gyrus (*51*), are regions known for early Aβ deposition, suggests that reactive astrogliosis, as detected with ^{18}F-SMBT-1, is associated with early Aβ deposition at the preclinical stages of AD and likely plays a moderating or modulating role over neurodegeneration, cognitive trajectories and clinical progression. This was further confirmed by the correlational and vertexwise analysis where ^{18}F-SMBT-1 binding in the same regions was highly correlated with Aβ. But the association between ^{18}F-SMBT-1 binding and Aβ merits to be examined more closely. The highest correlations were observed in areas of *early* Aβ deposition while in other areas, characterized by high Aβ like the frontal cortex, the correlations were much lower. In contrast, brain areas known for high density of MAO-B in the brain

presented either a lack of correlation, or even an inverse correlation as observed in MTL, anterior cingulate and basal ganglia. And while the association between ^{18}F-SMBT-1 binding and Aβ accumulation in areas like the inferior temporal follow a linear relationship, (Supplementary Figure 2) the association between ^{18}F-SMBT-1 binding and Aβ is better described by a non-linear fit that suggests that the increase in ^{18}F-SMBT-1 signal likely precedes Aβ becoming abnormal (Supplementary Figure 1) in agreement with the hypothesis that postulates reactive astrogliosis precede the significant build-up of Aβ plaques in the brain. (*24,53*) This suggests that astrocytes could be reactive and increase MAO-B expression/activity in response to Aβ changes which precede plaque deposition (e.g., increased brain concentration of Aβ oligomers and protofibrils). The high association of reactive astrogliosis with insoluble Aβ, coupled with its early manifestation has prompted to postulate that the neuroinflammatory *reaction* is driven by soluble Aβ oligomers. (*24,25*) As stated before, astrocytes do not constitute a homogenous population, and have -and adopt- different morphological, biochemical and functional properties reflecting a complex mix of toxic and protective pathways. (*6*) Thus, the relationship with Aβ -and tau-, given the diverse morphological and biochemical diversity of astrocytes, is not likely to be straightforward or the same across different brain regions, indicating a more complex and regional relationship rather than a global response.

The associations between ^{18}F-SMBT-1 binding and brain volumetrics or WMH were not strong. It is worth mentioning that hippocampal and parahippocampal ^{18}F-SMBT-1 binding were associated with HV, as ^{18}F-SMBT-1 binding in caudate, pallidus, thalamus and pons were also directly associated with GM volumes, but these were all direct associations where lower ^{18}F-SMBT-1 binding was associated with smaller volumes. The expedient explanation for all these regions would be that these regions –regions with normally high concentrations of MAO-B– are atrophic. As explained in the section dealing with the correlations with Aβ, the hippocampi in the Aβ+ AD group were significantly more atrophic, so the lower ^{18}F-SMBT-1 binding in the hippocampus and parahippocampal gyrus can be explained by PVE. But the basal ganglia were not atrophic and there were no significant differences across the groups, so PVE cannot explain the lower ^{18}F-SMBT-1 binding. We believe the results in the basal ganglia truly reflect a reduction of ^{18}F-SMBT-1 binding in these areas, especially in AD, where, as the neurodegeneration progresses the expression of MAO-B is likely decreasing, most noticeably in those areas with high density of MAO-B like the basal ganglia.

In regards to the associations between ^{18}F-SMBT-1 binding and cognitive parameters, it can be said that the main driver of cognitive impairment across all domains was tau burden, contributing >50%

of the variance, followed by HV. Sex was also contributing to Episodic Memory and AIBL PACC, with females performing worse than males. ^{18}F-SMBT-1 binding was mainly correlated with MMSE and AIBL PACC in some neocortical regions such the frontal cortex, with lateral temporal, supramarginal gyrus and angular gyrus, contributing 24-35% of the variance of MMSE, and 18-28% of the variance of AIBL PACC. These findings suggest that reactive astrogliosis has a detrimental contribution to general cognition and some memory tasks that are independent of tau, Aβ or hippocampal atrophy. This suggests that ameliorating neuroinflammation early on in the evolution of the disease, might be a potential complementary therapeutic avenue for AD (*20*).

There are several limitations and caveats that need to be considered in this study. In a similar fashion to microglial activation, only surrogate markers are available to assess reactive astrogliosis. In contrast to neuroreceptor PET studies that use tracers that bind directly to the receptor, the study of neuroinflammation is based on using surrogate markers to assess their change of state, from resting to activated. Thus microglial activation has been for decades studied assessing overexpression of mitochondrial Translocator Protein 18 kDa (*18*) and more recently tracers for macrophage colony-stimulating factor 1 receptor (*54*) or purinergic receptors (*55*) while reactive astrogliosis was assessed with markers of MAO-B (*19*) and imidazoline 2 binding sites (*29*) It needs to be clearly understood that ^{18}F-SMBT-1 is a MAO-B tracer, and as such, several factors and conditions that affect MAO-B can affect ^{18}F-SMBT-1 binding. Besides the obvious effect of MAO-B inhibitors, MAO-B also increases with age (*56*), it is affected by smoking (*57*) and has been found to be altered in psychiatric conditions such as major depression (*22*). Therefore, careful clinical anamnesis and itemized listing of exclusionary criteria are required before participants undergo a ^{18}F-SMBT-1 PET scan. While MAO-B is mainly present in astrocytes it is also found, in a much smaller concentration, in neurons. (*58*) ^{18}F-SMBT-1 can detect increases and decreases of MAO-B in the brain, but cannot discriminate between the fluid change and/or transition of reactive astrocytes from a protective to a toxic state, and not all reactive astrocytes overexpress MAO-B. (*58*) The small number of Aβ+ MCI precludes drawing any conclusion regarding group differences in the SMBT-1 signal. A larger sample size, especially Aβ+ MCI and Aβ+ AD patients, will be required to further validate the findings that ^{18}F-SMBT-1 captures the reported increases in MAO-B across the AD continuum. There is also a chance of spurious correlations derived from analyzing subgroups. These correlations were undertaken to dissect the relation between the different aspects of ^{18}F-SMBT-1 binding in the presence or absence of Aβ and tau, and how ^{18}F-SMBT-1 binding is related to other variables. Finally, the participants were volunteers who were not randomly selected from the community and were generally well educated and had high scores on cognitive tests, thus these findings might not be generalized to the general population.

The introduction of biomarker-based approaches for the identification of brain pathology has informed new strategies for the design of clinical trials aimed at preventing the onset of cognitive impairment and dementia. Markers of Aβ and tau pathology and markers of neurodegeneration have been incorporated into a recently proposed biomarker-based "framework" (*59*) The advantage of the modular design of the framework, and considering that reactive gliosis is a critical aspect of the neuropathology of AD, is that the biomarker framework might be expanded to include reactive gliosis.

Our studies showed ^{18}F-SMBT-1 can be used as surrogate marker of reactive astrogliosis where, despite the limited sample size in some of the groups, there was a distinctive degree and pattern of tracer binding across the AD continuum that was mainly associated with the presence of Aβ burden in the brain. ^{18}F-SMBT-1 will allow a better understanding of the pathophysiology of AD, enabling more accurate staging and prognosis at earlier stages of the disease. It will also be necessary to examine the relationship between ^{18}F-SMBT-1 binding in the brain and plasma GFAP. Longitudinal studies will be required to assess the effects of reactive astrogliosis over the clinical expression of AD and also, given the intimate relationship between astrocytes and bloods vessels, of cerebrovascular disease. It will also require longitudinal studies to fully elucidate the complex interaction between reactive astrogliosis, AD pathology and cerebrovascular disease and their moderating or modulating impact over neurodegeneration, cognitive decline and clinical progression.

CONCLUSIONS

Cross-sectional human PET studies with ^{18}F-SMBT-1, a highly selective F-18 labelled MAO-B tracer showed that Aβ+ AD, but most importantly, Aβ+ cognitively unimpaired controls have significantly higher regional ^{18}F-SMBT-1 binding than Aβ- CN. Moreover, in several regions of the brain, ^{18}F-SMBT-1 retention was highly associated with Aβ burden. These findings suggest that increased ^{18}F-SMBT-1 binding occurs at the preclinical stages of Aβ accumulation, providing strong support for its use as surrogate marker of astrogliosis and a biomarker of early stages in the Alzheimer's disease continuum.

ACKNOWLEDGEMENTS

The study was supported in part by National Health Medical Research Council (NHMRC) of Australia grants G1005121 and grant 19KK0212 from Japan. The funding sources had no input into the design of this study, the analysis of data, or writing of the manuscript.

The authors would like to thank the Brain Research Institute for support in acquiring the MRI data.

We would like to thank Dr Chester Mathis, Dr William E Klunk, Dr Oscar Lopez, Dr Ann Cohen, Dr Brian Lopresti, Dr Howard Aizenstein, Dr Scott Mason, Dr Beth Snitz and Dr Beth Shaaban at the University of Pittsburgh for extremely fruitful discussions around SMBT-1, MAO-B and reactive astrogliosis.

We thank the participants who took part in the study and their families

This paper is dedicated to my father, Victor E. Villemagne. 1/8/35-5/7/21

KEY POINTS:

QUESTION: Can ^{18}F-SMBT-1 be used to assess reactive astrogliosis in vivo?

PERTINENT FINDINGS: A clinical study in 77 elderly participants, showed that ^{18}F-SMBT-1, a novel F-18 MAO-B tracer used as a surrogate marker of reactive astrogliosis, was significantly higher in Alzheimer's disease patients, and most importantly, in cognitively unimpaired elderly controls with high Aβ in the brain.

IMPLICATIONS FOR PATIENT CARE: ^{18}F-SMBT-1 can be used as a surrogate and early marker of reactive astrogliosis across the Alzheimer's disease continuum.

REFERENCES

1. Masters CL. Neuropathology of Alzheimer's Disease. In: Burns A, O'Brien J, Ames D, eds. *Dementia (3rd Edition)*. London: Hodder Arnold; 2005:393-407.

2. Fakhoury M. Microglia and Astrocytes in Alzheimer's Disease: Implications for Therapy. *Curr Neuropharmacol.* 2018;16:508-518.

3. Vasile F, Dossi E, Rouach N. Human astrocytes: structure and functions in the healthy brain. *Brain Struct Funct.* 2017;222:2017-2029.

4. McConnell HL, Li Z, Woltjer RL, Mishra A. Astrocyte dysfunction and neurovascular impairment in neurological disorders: Correlation or causation? *Neurochem Int.* 2019;128:70-84.

5. Sofroniew MV. Astrogliosis. *Cold Spring Harb Perspect Biol.* 2014;7:a020420.

6. Escartin C, Galea E, Lakatos A, et al. Reactive astrocyte nomenclature, definitions, and future directions. *Nat Neurosci.* 2021;24:312-325.

7. Osborn LM, Kamphuis W, Wadman WJ, Hol EM. Astrogliosis: An integral player in the pathogenesis of Alzheimer's disease. *Prog Neurobiol.* 2016;144:121-141.

8. Carter SF, Herholz K, Rosa-Neto P, Pellerin L, Nordberg A, Zimmer ER. Astrocyte Biomarkers in Alzheimer's Disease. *Trends Mol Med.* 2019;25:77-95.

9. Birch AM. The contribution of astrocytes to Alzheimer's disease. *Biochem Soc Trans.* 2014;42:1316-1320.

10. Acioglu C, Li L, Elkabes S. Contribution of astrocytes to neuropathology of neurodegenerative diseases. *Brain Res.* 2021:147291.

11. Kovacs GG, Xie SX, Robinson JL, et al. Sequential stages and distribution patterns of aging-related tau astrogliopathy (ARTAG) in the human brain. *Acta Neuropathol Commun.* 2018;6:50.

12. Nelson PT, Dickson DW, Trojanowski JQ, et al. Limbic-predominant age-related TDP-43 encephalopathy (LATE): consensus working group report. *Brain.* 2019;142:1503-1527.

13. Yamanaka K, Komine O. The multi-dimensional roles of astrocytes in ALS. *Neurosci Res.* 2018;126:31-38.

14. Radford RA, Morsch M, Rayner SL, Cole NJ, Pountney DL, Chung RS. The established and emerging roles of astrocytes and microglia in amyotrophic lateral sclerosis and frontotemporal dementia. *Front Cell Neurosci.* 2015;9:414.

15. Engler H, Nennesmo I, Kumlien E, et al. Imaging astrocytosis with PET in Creutzfeldt-Jakob disease: case report with histopathological findings. *Int J Clin Exp Med.* 2012;5:201-207.

16. Diniz LP, Araujo APB, Matias I, et al. Astrocyte glutamate transporters are increased in an early sporadic model of synucleinopathy. *Neurochem Int.* 2020;138:104758.

17. Ingelsson M, Fukumoto H, Newell KL, et al. Early Abeta accumulation and progressive synaptic loss, gliosis, and tangle formation in AD brain. *Neurology.* 2004;62:925-931.

18. Kreisl WC, Lyoo CH, Liow JS, et al. (11)C-PBR28 binding to translocator protein increases with progression of Alzheimer's disease. *Neurobiol Aging.* 2016;44:53-61.

19. Carter SF, Scholl M, Almkvist O, et al. Evidence for astrocytosis in prodromal Alzheimer disease provided by 11C-deuterium-L-deprenyl: a multitracer PET paradigm combining 11C-Pittsburgh compound B and 18F-FDG. *J Nucl Med.* 2012;53:37-46.

20. Assefa BT, Gebre AK, Altaye BM. Reactive Astrocytes as Drug Target in Alzheimer's Disease. *Biomed Res Int.* 2018;2018:4160247.

21. Ekblom J, Jossan SS, Bergstrom M, Oreland L, Walum E, Aquilonius SM. Monoamine oxidase-B in astrocytes. *Glia.* 1993;8:122-132.

22. Moriguchi S, Wilson AA, Miler L, et al. Monoamine Oxidase B Total Distribution Volume in the Prefrontal Cortex of Major Depressive Disorder: An [11C]SL25.1188 Positron Emission Tomography Study. *JAMA Psychiatry.* 2019;76:634-641.

23. Saba W, Valette H, Peyronneau MA, et al. [(11)C]SL25.1188, a new reversible radioligand to study the monoamine oxidase type B with PET: preclinical characterisation in nonhuman primate. *Synapse.* 2010;64:61-69.

24. Rodriguez-Vieitez E, Ni R, Gulyas B, et al. Astrocytosis precedes amyloid plaque deposition in Alzheimer APPswe transgenic mouse brain: a correlative positron emission tomography and in vitro imaging study. *Eur J Nucl Med Mol Imaging.* 2015;42:1119-1132.

25. Rodriguez-Vieitez E, Saint-Aubert L, Carter SF, et al. Diverging longitudinal changes in astrocytosis and amyloid PET in autosomal dominant Alzheimer's disease. *Brain.* 2016;139:922-936.

26. Scholl M, Carter SF, Westman E, et al. Early astrocytosis in autosomal dominant Alzheimer's disease measured in vivo by multi-tracer positron emission tomography. *Sci Rep.* 2015;5:16404.

27. Kumar A, Koistinen NA, Malarte ML, et al. Astroglial tracer BU99008 detects multiple binding sites in Alzheimer's disease brain. *Mol Psychiatry.* 2021.

28. Venkataraman AV, Keat N, Myers JF, et al. First evaluation of PET-based human biodistribution and radiation dosimetry of (11)C-BU99008, a tracer for imaging the imidazoline2 binding site. *EJNMMI Res.* 2018;8:71.

29. Calsolaro V, Matthews PM, Donat CK, et al. Astrocyte reactivity with late-onset cognitive impairment assessed in vivo using (11)C-BU99008 PET and its relationship with amyloid load. *Mol Psychiatry.* 2021.

30. Harada R, Hayakawa Y, Ezura M, et al. (18)F-SMBT-1: A Selective and Reversible PET Tracer for Monoamine Oxidase-B Imaging. *J Nucl Med.* 2021;62:253-258.

31. Villemagne VL, Harada H, Doré V, et al. First-in-human evaluation of 18F-SMBT-1, a novel 18F-labeled MAO-B PET tracer for imaging reactive astrogliosis. *J Nucl Med.* 2022;(In Press).

32. Petersen RC, Smith GE, Waring SC, Ivnik RJ, Tangalos EG, Kokmen E. Mild cognitive impairment: clinical characterization and outcome. *Arch Neurol.* 1999;56:303-308.

33. McKhann GM, Knopman DS, Chertkow H, et al. The diagnosis of dementia due to Alzheimer's disease: Recommendations from the National Institute on Aging-Alzheimer's Association workgroups on diagnostic guidelines for Alzheimer's disease. *Alzheimers Dement.* 2011;7:263-269.

34. Rowe CC, Jones G, Dore V, et al. Standardized Expression of 18F-NAV4694 and 11C-PiB beta-Amyloid PET Results with the Centiloid Scale. *J Nucl Med.* 2016;57:1233-1237.

35. Navitsky M, Joshi AD, Kennedy I, et al. Standardization of amyloid quantitation with florbetapir standardized uptake value ratios to the Centiloid scale. *Alzheimers Dement.* 2018;14:1565-1571.

36. Klunk WE, Koeppe RA, Price JC, et al. The Centiloid Project: standardizing quantitative amyloid plaque estimation by PET. *Alzheimers Dement.* 2015;11:1-15 e11-14.

37. Battle MR, Pillay LC, Lowe VJ, et al. Centiloid scaling for quantification of brain amyloid with [(18)F]flutemetamol using multiple processing methods. *EJNMMI Res.* 2018;8:107.

38. Bourgeat P, Dore V, Fripp J, et al. Implementing the centiloid transformation for (11)C-PiB and beta-amyloid (18)F-PET tracers using CapAIBL. *Neuroimage.* 2018;183:387-393.

39. Villemagne VL, Burnham S, Bourgeat P, et al. Amyloid beta deposition, neurodegeneration, and cognitive decline in sporadic Alzheimer's disease: a prospective cohort study. *Lancet Neurol.* 2013;12:357-367.

40. Krishnadas N, Dore V, Lamb F, et al. Case Report: (18)F-MK6240 Tau Positron Emission Tomography Pattern Resembling Chronic Traumatic Encephalopathy in a Retired Australian Rules Football Player. *Front Neurol.* 2020;11:598980.

41. Brendel M, Barthel H, van Eimeren T, et al. Assessment of 18F-PI-2620 as a Biomarker in Progressive Supranuclear Palsy. *JAMA Neurol.* 2020;77:1408-1419.

42. Jack CR, Jr., Wiste HJ, Schwarz CG, et al. Longitudinal tau PET in ageing and Alzheimer's disease. *Brain.* 2018;141:1517-1528.

43. Jack CR, Jr., Wiste HJ, Weigand SD, et al. Defining imaging biomarker cut points for brain aging and Alzheimer's disease. *Alzheimers Dement.* 2017;13:205-216.

44. Van Leemput K, Maes F, Vandermeulen D, Suetens P. Automated model-based tissue classification of MR images of the brain. *IEEE Trans Med Imaging.* 1999;18:897-908.

45. Boccardi M, Bocchetta M, Apostolova LG, et al. Delphi definition of the EADC-ADNI Harmonized Protocol for hippocampal segmentation on magnetic resonance. *Alzheimers Dement.* 2015;11:126-138.

46. Manjón JV, Coupé P, Raniga P, Xia Y, Fripp J, Salvado O. HIST: hyperintensity segmentation tool. Paper presented at: International Workshop on Patch-based Techniques in Medical Imaging, 2016.

47. Chatterjee P, Pedrini S, Stoops E, et al. Plasma glial fibrillary acidic protein is elevated in cognitively normal older adults at risk of Alzheimer's disease. *Transl Psychiatry.* 2021;11:27.

48. Cicognola C, Janelidze S, Hertze J, et al. Plasma glial fibrillary acidic protein detects Alzheimer pathology and predicts future conversion to Alzheimer dementia in patients with mild cognitive impairment. *Alzheimers Res Ther.* 2021;13:68.

49. Gulyas B, Pavlova E, Kasa P, et al. Activated MAO-B in the brain of Alzheimer patients, demonstrated by [11C]-L-deprenyl using whole hemisphere autoradiography. *Neurochem Int.* 2011;58:60-68.

50. Smale G, Nichols NR, Brady DR, Finch CE, Horton WE, Jr. Evidence for apoptotic cell death in Alzheimer's disease. *Exp Neurol.* 1995;133:225-230.

51. Villain N, Chetelat G, Grassiot B, et al. Regional dynamics of amyloid-beta deposition in healthy elderly, mild cognitive impairment and Alzheimer's disease: a voxelwise PiB-PET longitudinal study. *Brain.* 2012;135:2126-2139.

52. Guo T, Landau SM, Jagust WJ, Alzheimer's Disease Neuroimaging I. Detecting earlier stages of amyloid deposition using PET in cognitively normal elderly adults. *Neurology.* 2020;94:e1512-e1524.

53. Leclerc B, Abulrob A. Perspectives in molecular imaging using staging biomarkers and immunotherapies in Alzheimer's disease. *ScientificWorldJournal.* 2013;2013:589308.

54. Horti AG, Naik R, Foss CA, et al. PET imaging of microglia by targeting macrophage colony-stimulating factor 1 receptor (CSF1R). *Proc Natl Acad Sci U S A.* 2019;116:1686-1691.

55. Beaino W, Janssen B, Kooij G, et al. Purinergic receptors P2Y12R and P2X7R: potential targets for PET imaging of microglia phenotypes in multiple sclerosis. *J Neuroinflammation.* 2017;14:259.

56. Galva MD, Bondiolotti GP, Olasmaa M, Picotti GB. Effect of aging on lazabemide binding, monoamine oxidase activity and monoamine metabolites in human frontal cortex. *J Neural Transm Gen Sect.* 1995;101:83-94.

57. Fowler JS, Volkow ND, Wang GJ, et al. Neuropharmacological actions of cigarette smoke: brain monoamine oxidase B (MAO B) inhibition. *J Addict Dis.* 1998;17:23-34.

58. Perez-Nievas BG, Serrano-Pozo A. Deciphering the Astrocyte Reaction in Alzheimer's Disease. *Front Aging Neurosci.* 2018;10:114.

59. Jack CR, Jr., Bennett DA, Blennow K, et al. A/T/N: An unbiased descriptive classification scheme for Alzheimer disease biomarkers. *Neurology.* 2016;87:539-547.

Figure Legends

Figure 1. ^{18}F-SMBT-1 in elderly controls and across the AD spectrum

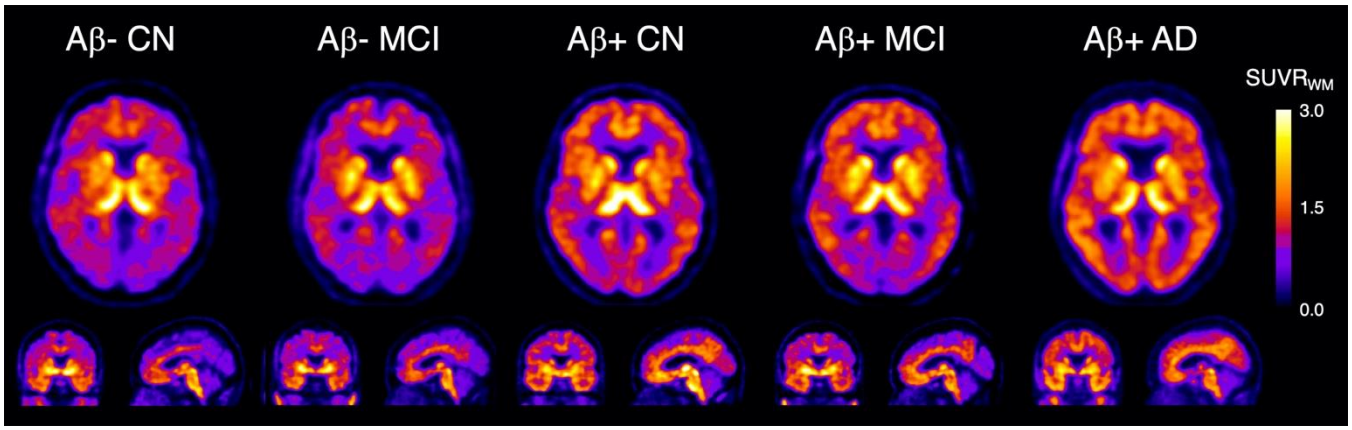

Representative transaxial, coronal and sagittal ^{18}F-SMBT-1 PET images in an Aβ- cognitively unimpaired control (Aβ- CN, 84 yo M, MMSE 28, CDR 0, 7 CL); an Aβ- mild cognitively impaired (Aβ- MCI, 69 yo F, MMSE 27, CDR 0.5, 9 CL); Aβ+ cognitively unimpaired control (Aβ+ CN, 72 yo M, MMSE 29, CDR 0, 24 CL); an Aβ+ mild cognitively impaired (Aβ+ MCI, 72 yo M, MMSE 27, CDR 0.5, 144 CL); and an Aβ+ Alzheimer's disease patient (Aβ+ AD, 78 yo F, MMSE 25, CDR 1, 173 CL).

In Aβ- CN and MCI it can be observed the normal distribution of ^{18}F-SMBT-1 in the brain, highlighting cortical areas with high concentration of MAO-B such as the basal ganglia, thalamus, mesial temporal cortex and anterior cingulate, as well as the different nuclei in the brainstem. Higher cortical ^{18}F-SMBT-1 binding is observed in Aβ+ CN, MCI and AD participants, with binding extending to frontal, temporal, occipital and posterior cingulate.

Abbreviations: CN (age-matched control); AD (Alzheimer's disease); SUVR$_{WM}$ (Standard Uptake Value Ratio using White Matter as reference region); CL (Centiloids).

Figure 2. Regional ^{18}F-SMBT-1 binding in elderly controls and across the AD spectrum

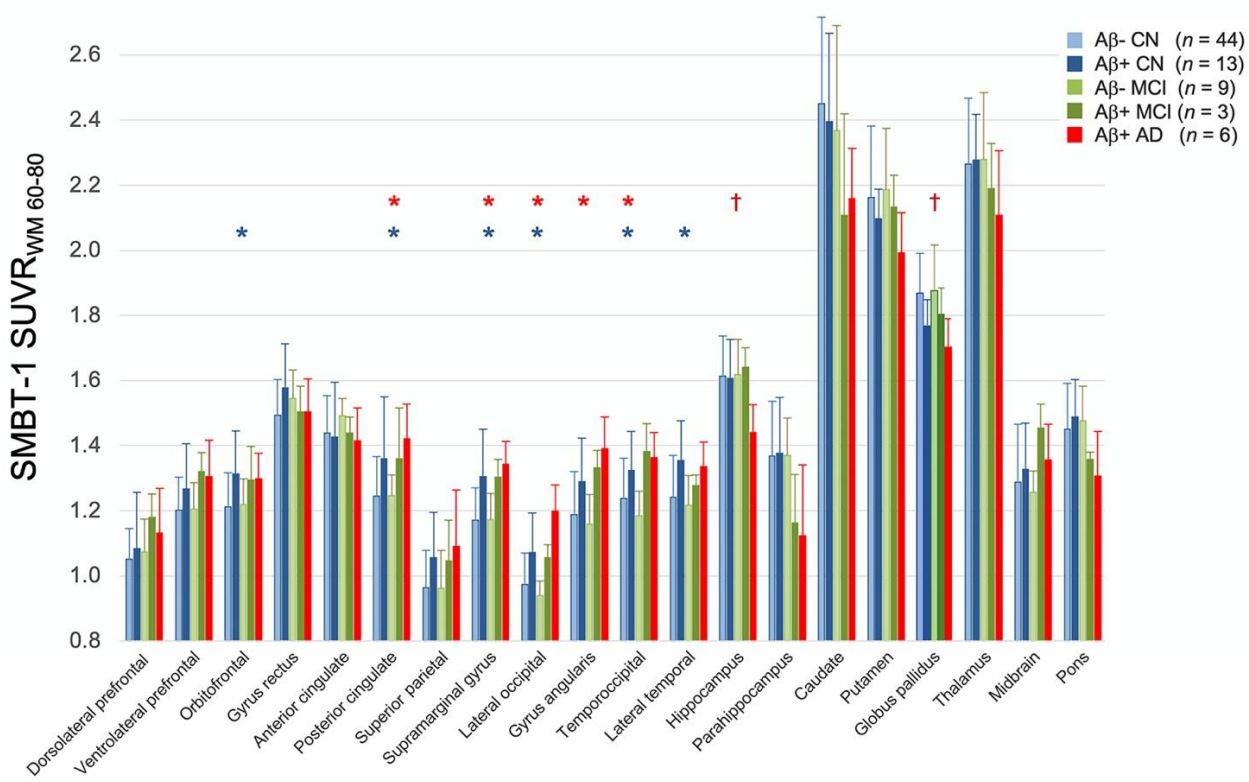

Bar graphs showing regional ^{18}F-SMBT-1 SUVR was significantly higher in posterior cingulate, supramarginal gyrus, lateral occipital, gyrus angularis and primary visual cortex in the Aβ+ AD group, but also was significantly lower in globus pallidus and hippocampus. In addition to posterior cingulate, supramarginal gyrus, and lateral occipital, ^{18}F-SMBT-1 binding was also significantly higher in orbitofrontal, lateral and inferior temporal gyri, and also significantly lower in the globus pallidus. Similar regions, like the supramarginal gyrus, showed higher ^{18}F-SMBT-1 binding in the Aβ+ MCI group, but none reached significance.

* *Significantly higher than Aβ- CN (p<0.05)*

† *Significantly lower than Aβ- CN (p<0.05)*

Abbreviations: CN (age-matched control); AD (Alzheimer's disease); $SUVR_{WM}$ (Standard Uptake Value Ratio using White Matter as reference region)

Figure 3. Vertexwise association between ^{18}F-SMBT-1 binding, Aβ and tau

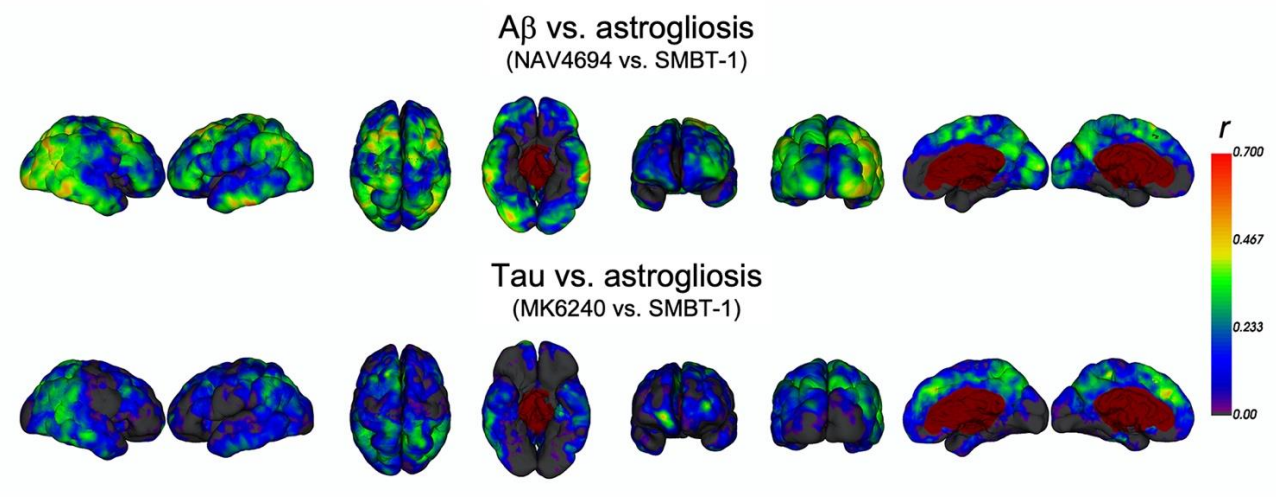

Positive vertex-wise associations between ^{18}F-SMBT-1 binding and Aβ. **(A)** There were high regional associations between ^{18}F-SMBT-1 binding and Aβ across the brain areas of early Aβ deposition such as temporoparietal, supramarginal and posterior cingulate, but also much lower associations were observed in areas also characterized by high Aβ, such as the frontal lobe and superior temporal gyrus. Some areas, particularly those characterized by high MAO-B concentrations in Aβ- CN, like the basal ganglia, the MTL and anterior cingulate, presented negative correlations (not shown).

Much less extensive regional associations were observed with tau **(B)**

The color scale represents the regression coefficients (*r*)

Graphical Abstract

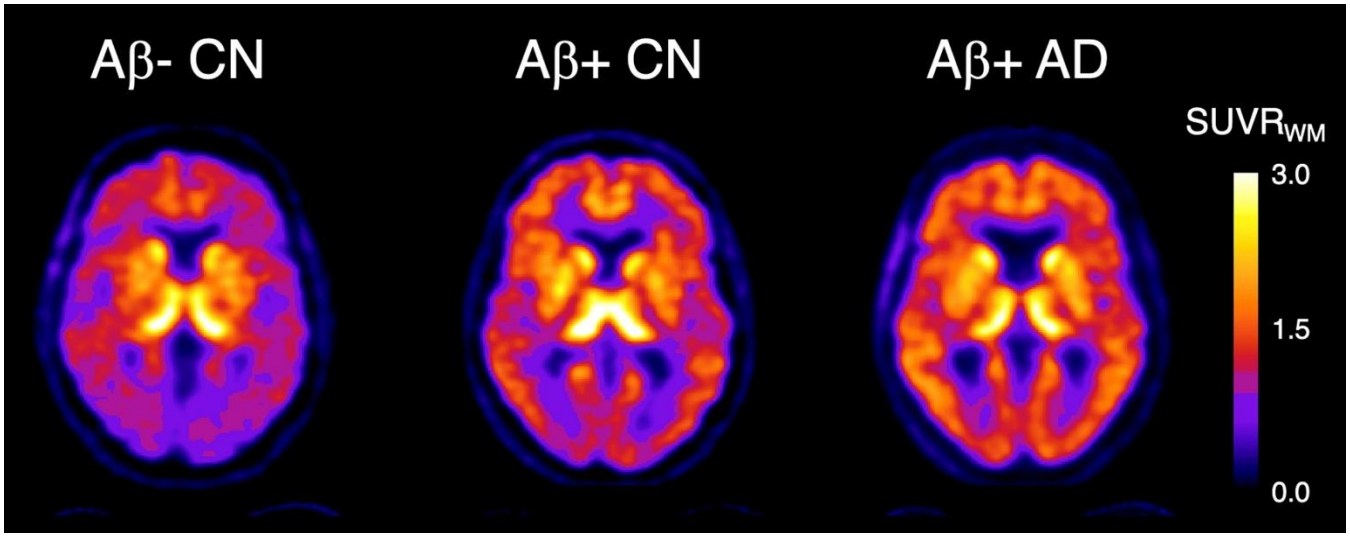

TABLE 1. Demographics

	CN	MCI	AD
n	57	12	8
Age	76.8±5.1	73.4±5.8	76.4±7.6
Sex	32F/25M	4F/8M*	5F/3M
Education (years)	14.8±2.7	10.0±1.7*	10.3±1.3*
%APOE4	39%	25%	57%*
MMSE	28.6±1.5	27.9±1.7	24.1±4.1*
CDR	0.03±0.1	0.33±0.3*	0.69±0.3*
CDR SoB	0.05±0.2	0.46±0.3	6.00±2.3*
Episodic Memory	0.16±0.8	-1.08±0.5*	-3.40±1.5*
Non-Memory	-0.06±0.6	-0.86±0.5*	-2.61±1.8*
AIBL PACC	0.09±0.6	-0.85±0.7*	-4.25±2.0*
Hippocampus (cc)	5.91±0.5	5.80±0.8	4.84±0.7*
Cortical Grey Matter (cc)	467±35	467±10	429±22*
White Matter (cc)	388±26	388±17	387±28
Ventricles (cc)	33.8±13	37.0±25	43.5±13
White Matter Hyperintensities (cc)	5.15±6.6	4.60±7.1	17.8±19*
Aβ burden (CL)	13.7±33	20.3±43	85.8±66*
Aβ accumulation (CL/yr, *n=31*)	2.35±4.1	0.22±0.1	4.08
Tau Me (SUVR)	0.95±0.2	1.14±0.3	1.58±1.0*
Tau Te (SUVR)	1.05±0.2	1.20±0.2	1.93±1.2*
Tau R (SUVR)	0.90±0.1	1.01±0.1	1.49±0.7*
Tau Meta-Temporal (SUVR)	1.03±0.2	1.21±0.3	1.83±1.2*
%Aβ+	23%	25%	75%*
%Tau+	18%	42%	67%*

Abbreviations
CN: elderly controls; MCI: mild cognitive impairment; AD: Alzheimer's disease; MMSE: Mini mental State Examination; CDR: Clinical Dementia Rating; CDR SoB: Clinical Dementia Rating Sum of Boxes; AIBL PACC: the Australian Imaging Biomarkers and Lifestyle's Preclinical Alzheimer Cognitive Composite. Me: Mesial Temporal; Te: Temporoparietal; R: Rest of neocortex.

* *Significantly different from controls (p<0.05)*

TABLE 2. Association between regional ^{18}F-SMBT-1 binding and global Aβ burden, meta-temporal tau and Aβ accumulation

	Centiloids (n=77)		Meta-temporal Tau SUVR (n=72)		Aβ accumulation [CL/yr] (n=31)	
REGION SMBT-1	**r**	***p***	**r**	***p***	**r**	***p***
Ventrolateral Prefrontal	0.180	*(p=0.117)*	0.130	*(p=0.281)*	0.177	*(p=0.341)*
Orbitofrontal	0.233	***(p=0.042)***	0.137	*(p=0.254)*	0.240	*(p=0.193)*
Anterior Cingulate	-0.127	*(p=0.270)*	0.079	*(p=0.513)*	-0.017	*(p=0.926)*
Posterior Cingulate	0.339	***(p=0.003)***	0.339	***(p=0.004)***	0.212	*(p=0.253)*
Superior Parietal	0.230	***(p=0.044)***	0.283	***(p=0.017)***	0.159	*(p=0.393)*
Supramarginal Gyrus	0.477	***(p<.0001)***	0.365	***(p=0.002)***	0.315	*(p=0.084)*
Lateral Occipital	0.484	***(p<.0001)***	0.308	***(p=0.009)***	0.297	*(p=0.105)*
Primary Visual Cortex	0.322	***(p=0.004)***	0.229	*(p=0.055)*	0.049	*(p=0.794)*
Gyrus Angularis	0.382	***(p=0.001)***	0.280	***(p=0.018)***	0.271	*(p=0.141)*
Temporoccipital	0.334	***(p=0.003)***	0.306	***(p=0.010)***	0.340	*(p=0.061)*
Lateral Temporal	0.275	***(p=0.015)***	0.194	*(p=0.106)*	0.431	***(p=0.016)***
Inferior Temporal	0.233	***(p=0.042)***	-0.073	*(p=0.543)*	0.668	***(p<.0001)***
Amygdala	-0.081	*(p=0.482)*	-0.145	*(p=0.229)*	0.290	*(p=0.114)*
Hippocampus	-0.170	*(p=0.140)*	-0.114	*(p=0.343)*	0.240	*(p=0.193)*
Parahippocampus	-0.161	*(p=0.161)*	-0.122	*(p=0.310)*	0.363	*(p=0.051)*
Entorhinal Cortex	-0.062	*(p=0.595)*	-0.119	*(p=0.323)*	-0.035	*(p=0.850)*
Caudate Nuclei	-0.248	***(p=0.030)***	-0.262	***(p=0.027)***	0.172	*(p=0.356)*
Putamen	-0.235	***(p=0.040)***	-0.211	*(p=0.078)*	-0.100	*(p=0.593)*
Globus Pallidus	-0.432	***(p<.0001)***	-0.391	***(p=0.001)***	-0.249	*(p=0.176)*
Thalamus	-0.179	*(p=0.120)*	-0.215	*(p=0.072)*	-0.139	*(p=0.457)*
Midbrain	0.185	*(p=0.108)*	0.183	*(p=0.128)*	0.086	*(p=0.644)*
Pons	-0.146	*(p=0.205)*	-0.203	*(p=0.090)*	0.310	*(p=0.090)*

Abbreviations: SUVR: Standard Uptake Value Ratio. CL: Centiloids

Bolded fonts *Significant associations (p<0.05)*

TABLE 3. Association between regional ^{18}F-SMBT-1 binding and cognitive performance

	MMSE		CDR SoB		Episodic Memory		Non-Memory		AIBL PACC	
SMBT-1 Region	β	***p***	β	***p***	β	***p***	β	***p***	β	***p***
Ventrolateral Prefrontal	**-0.27**	***0.025***	0.16	*0.109*	-0.12	*0.240*	-0.12	*0.286*	**-0.21**	***0.032***
Orbitofrontal	**-0.35**	***0.004***	0.14	*0.168*	-0.11	*0.313*	-0.12	*0.285*	**-0.22**	***0.027***
Anterior Cingulate	**-0.25**	***0.036***	0.06	*0.545*	**-0.21**	***0.040***	-0.19	*0.084*	**-0.26**	***0.005***
Posterior Cingulate	-0.22	*0.082*	0.15	*0.150*	-0.07	*0.529*	-0.17	*0.136*	-0.19	*0.060*
Superior Parietal	-0.19	*0.124*	0.14	*0.175*	-0.00	*0.979*	-0.20	*0.072*	-0.15	*0.138*
Supramarginal Gyrus	**-0.29**	***0.025***	0.08	*0.479*	-0.09	*0.450*	-0.18	*0.127*	-0.17	*0.099*
Lateral Occipital	-0.17	*0.188*	**0.24**	***0.026***	-0.13	*0.252*	-0.14	*0.226*	**-0.21**	***0.046***
Gyrus Angularis	**-0.30**	***0.018***	0.16	*0.125*	-0.12	*0.266*	-0.14	*0.230*	-0.20	*0.051*
Temporoccipital	-0.17	*0.196*	0.01	*0.963*	-0.09	*0.422*	-0.03	*0.780*	-0.09	*0.406*
Lateral Temporal	**-0.35**	***0.003***	0.04	*0.689*	-0.14	*0.169*	-0.11	*0.293*	**-0.19**	***0.048***
Inferior Temporal	-0.22	*0.102*	0.20	*0.068*	**-0.25**	***0.023***	-0.08	*0.487*	**-0.28**	***0.007***
Amygdala	**-0.24**	***0.037***	0.10	*0.305*	-0.12	*0.240*	-0.20	*0.056*	**-0.20**	***0.032***
Hippocampus	-0.22	*0.072*	0.11	*0.304*	-0.17	*0.115*	-0.19	*0.092*	-0.18	*0.073*
Parahippocampus	-0.10	*0.420*	0.12	*0.217*	-0.01	*0.912*	-0.01	*0.922*	-0.07	*0.451*
Caudate	-0.01	*0.945*	-0.01	*0.912*	0.06	*0.604*	0.10	*0.358*	0.07	*0.518*
Putamen	-0.16	*0.207*	-0.07	*0.535*	-0.00	*0.996*	0.09	*0.240*	0.05	*0. 652*
Globus Pallidus	-0.02	*0.856*	-0.01	*0.904*	-0.20	*0.068*	-0.17	*0.150*	-0.14	*0.179*
Thalamus	-0.09	*0.473*	0.05	*0.657*	-0.06	*0.601*	-0.05	*0.631*	-0.09	*0.388*

Abbreviations
MMSE: Mini mental State Examination; CDR: Clinical Dementia Rating; CDR SoB: Clinical Dementia Rating Sum of Boxes; AIBL PACC: the Australian Imaging Biomarkers and Lifestyle's Preclinical Alzheimer Cognitive Composite.

Bolded fonts *Significant associations (p<0.05)*

SUPPLEMENTARY MATERIALS

Neuropsychological evaluation

Participants were administered the Mini Mental State Examination (MMSE), the Clinical Dementia Rating (CDR), Geriatric Depression Scale (GDS), Hospital Anxiety and Depression Scale (HADS), and a battery of neuropsychological tests. The primary cognitive performance measures were the composite memory and non-memory scores, and the AIBL-PACC score that were calculated as previously described.(*1,2*) Briefly, we calculated a composite episodic memory score from the mean of the z-scores (means and standard deviation for creating the z-scores were generated using data from 65 cognitively normal controls with both low ^{11}C-PiB PET retention and normal MRI as the reference) for Rey complex figure test (RCFT, 30 min) long delay, the delayed recall from the California verbal learning test second edition (CVLT-II), and Logical Memory II. We calculated a composite non-memory score by taking the mean of the z scores for the Boston naming test, letter fluency, category fluency, digit span forwards and backwards, digit symbol-coding, and RCFT copy. (*1*) The AIBL-PACC score was calculated from the mean of the z-scores of the delayed recall from CVLT-II and Logical Memory II, the digit symbol substitution Test and the MMSE total score. (*2*)

Supplementary Figure 1. Correlation between ^{18}F-SMBT-1 binding and Aβ burden

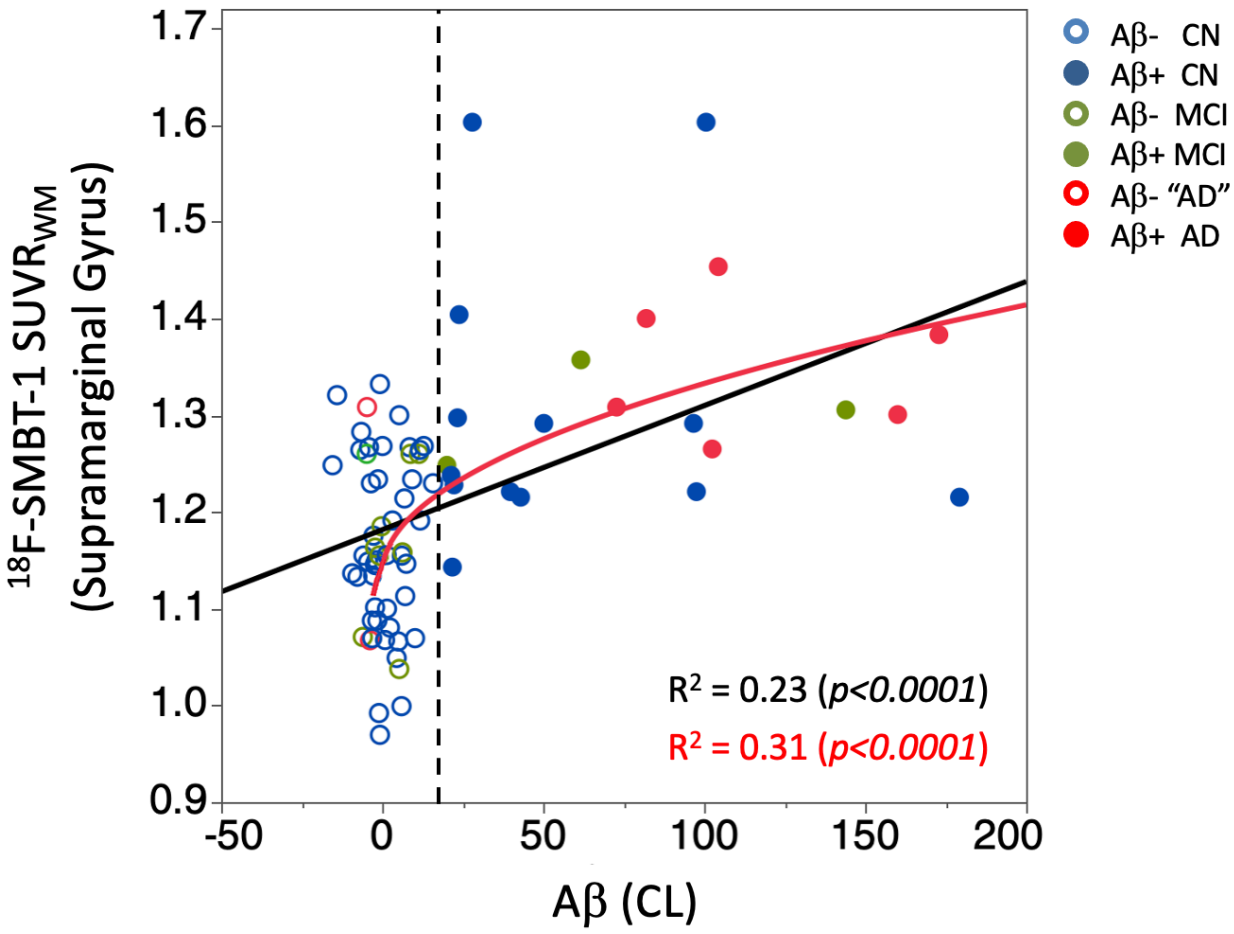

Linear and non-linear associations between ^{18}F-SMBT-1 binding in the supramarginal gyrus and global Aβ burden. The non-linear fit better described the relationship between ^{18}F-SMBT-1 binding and Aβ burden, suggesting that the ^{18}F-SMBT-1 signal starts increasing before Aβ becomes abnormal.

The dotted line denotes the 20 CL use to separate high from low Aβ.

Linear fit: y = a + b*x

Square root fit: y = a + b*Sqrt(x)

Supplementary Figure 2. Correlation between ^{18}F-SMBT-1 binding and Aβ accumulation

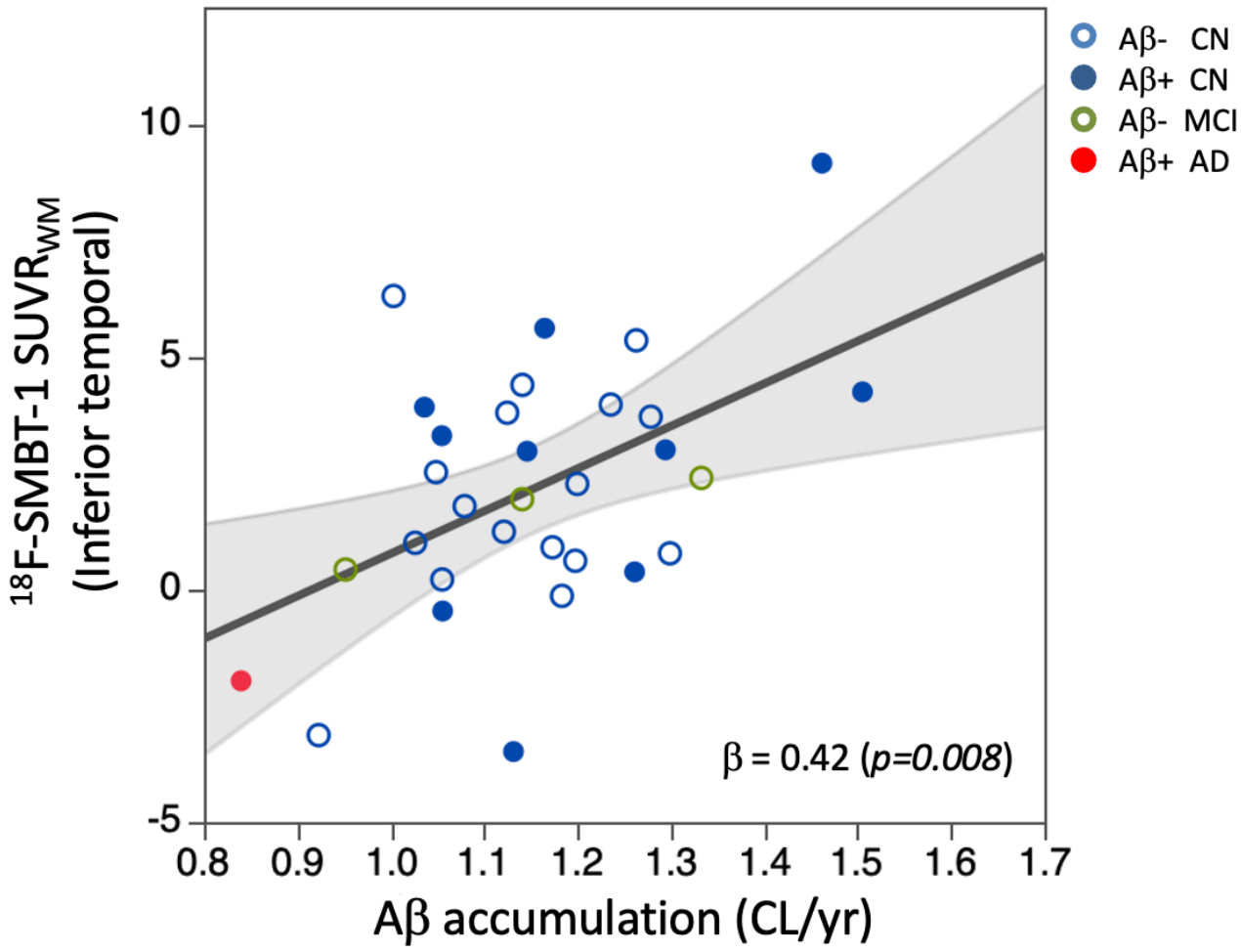

Linear association between ^{18}F-SMBT-1 binding in the inferior temporal and global rates of Aβ accumulation in 31 participants (1 Aβ+ AD, 3 Aβ- MCI, 17 Aβ- and 10 Aβ+ CN) with available Aβ imaging longitudinal data. The association suggests that the ^{18}F-SMBT-1 signal in the inferior temporal is higher on those participants with higher rates of Aβ accumulation. Association was adjusted for age, sex and baseline Aβ burden.

SUPPLEMENTARY TABLE 1. Demographics of cognitively unimpaired controls (CN) and Alzheimer's disease (AD) patients by amyloid status

	Aβ- CN	Aβ+ CN	Aβ- MCI	Aβ+ MCI	Aβ- AD	Aβ+ AD
n	44	13	9	3	2	6
Age	76.0±4.8	78.9±5.5	72.8±6.6	75.1±2.8	66.5±3.5	79.7±4.8
Sex	25F/19M	7F/6M	4F/5M	0F/3M	1F/1M	4F/2M
Education (years)	14.8±2.7	14.7±3.2	10.0±1.7*	11.7±4.2	10.9±1.8	10.3±1.3*
%APOE4	30%	69%*	22%	33%	0%	80%*
MMSE	28.6±1.5	28.6±1.6	28.4±1.7	26.3±0.6*	26.0±1.4	23.5±4.6*
CDR	0.05±0.1	0.00±0.0	0.28±0.3*	0.50±0.0*	0.75±0.4	0.67±0.3*
CDR SoB	0.07±0.2	0.00±0.0	0.39±0.3*	0.67±0.3*	4.50±0.7	6.50±2.4*
Episodic Memory	0.12±0.9	0.28±0.6	-1.03±0.5*	-1.19±0.5*	-1.96±0.0*	-3.58±1.5*
Non-Memory	-0.07±0.6	-0.04±0.7	-0.90±0.6*	-0.76±0.2*	-0.90±0.1*	-2.90±1.8*
AIBL PACC	0.07±0.7	0.15±0.6*	-0.76±0.7*	-1.11±0.4*	-2.56±0.0*	-4.53±2.1*
Hippocampus (cc)	5.94±0.5	5.83±0.4	5.81±0.9	5.73±0.8	5.71±0.2	4.50±0.5*
Cortical GM (cc)	472±38	452±14	468±10	465±14	452±27	419±13*
WM (cc)	387±27	390±22	388±18	383±17	381±52	390±19
Ventricles (cc)	34.0±15	33.0±7	35.1±22	42.0±38	39.6±19	45.0±12
WMH (cc)	5.41±6.9	4.25±5.6	4.54±7.8	4.79±6.0	5.44±6	22.7±21*
Aβ burden (CL)	0.79±6.9	57.5±48*	1.96±6.2	75.3±63*	-4.25±0.6	116±41*
Aβ accumulation (CL/yr)	0.61±2.6	5.32±4.6*	-0.22±0.1	-	-	4.08
Tau Me (SUVR)	0.89±0.2	1.16±0.2*	1.00±0.1	1.58±0.4*	0.88±0.3	2.05±1.1*
Tau Te (SUVR)	1.02±0.2	1.13±0.1	1.13±0.1	1.42±0.2*	1.06±0.2	2.52±1.2*
Tau R (SUVR)	0.90±0.1	0.93±0.1	0.98±0.1	1.10±0.0*	0.97±0.3	1.84±0.8*
Tau MT (SUVR)	0.98±0.2	1.18±0.2	1.10±0.1	1.56±0.3	1.00±0.3	2.39±1.3*
%Tau+	9%	46%*	22%*	100%*	50%*	75%*

Abbreviations

CN: elderly controls; MCI: mild cognitive impairment; AD: Alzheimer's disease; APOE: Apolipoprotein E; MMSE: Mini mental State Examination; CDR: Clinical Dementia Rating; CDR SoB: Clinical Dementia Rating Sum of Boxes; AIBL PACC: the Australian Imaging Biomarkers and Lifestyle's Preclinical Alzheimer Cognitive Composite. GM: Grey matter; WM: White Matter; WMH: White Matter Hyperintensities; SUVR: Standard Uptake Value Ratio. CL: Centiloids; Me: Mesial Temporal; Te: Temporoparietal; MT: Meta temporal; R: Rest of neocortex.

** Significantly different from Aβ- controls(p<0.05)*

SUPPL TABLE 2. Regional ^{18}F-SMBT-1 SUVR across clinical groups stratifies by Aβ status

	Aβ- CN SUVR$_{WM}$ (n=44)	Aβ+ CN SUVR$_{WM}$ (n=13)	*d*	Aβ- MCI SUVR$_{WM}$ (n=9)	*d*	Aβ+ MCI SUVR$_{WM}$ (n=3)	*d*	Aβ- "AD" SUVR$_{WM}$ (n=2)	Aβ+ AD SUVR$_{WM}$ (n=6)	*d*
Dorsolateral Prefrontal	1.05 ± 0.09	1.08 ± 0.17	*0.22*	1.07 ± 0.10	*0.21*	1.18 ± 0.07	*1.61*	1.10 ± 0.19	1.13 ± 0.14	*0.68*
Ventrolateral Prefrontal	1.20 ± 0.10	1.27 ± 0.14	*0.58*	1.21 ± 0.08	*0.11*	1.32 ± 0.06	*1.46*	1.26 ± 0.16	1.30 ± 0.11	*0.95*
Orbitofrontal	1.21 ± 0.10	**1.31 ± 0.13**	*0.86*	1.22 ± 0.08	*0.11*	1.29 ± 0.10	*0.80*	1.30 ± 0.13	1.30 ± 0.08	*0.99*
Anterior Cingulate	1.44 ± 0.12	1.43 ± 0.17	*-0.07*	1.49 ± 0.05	*0.54*	1.44 ± 0.05	*0.00*	1.46 ± 0.08	1.41 ± 0.10	*-0.27*
Posterior Cingulate	1.24 ± 0.12	**1.36 ± 0.19**	*0.76*	1.25 ± 0.06	*0.11*	1.36 ± 0.16	*0.85*	1.32 ± 0.20	**1.42 ± 0.11**	*1.56*
Superior Parietal	0.96 ± 0.12	1.06 ± 0.14	*0.77*	0.96 ± 0.12	*0.00*	1.05 ± 0.12	*0.75*	1.06 ± 0.17	1.10 ± 0.17	*0.95*
Supramarginal Gyrus	1.16 ± 0.09	**1.31 ± 0.15**	*1.21*	1.17 ± 0.08	*0.12*	1.30 ± 0.05	*1.92*	1.19 ± 0.17	**1.35 ± 0.07**	*2.36*
Lateral Occipital	0.97 ± 0.10	**1.07 ± 0.12**	*0.91*	0.94 ± 0.05	*-0.38*	1.06 ± 0.04	*1.18*	1.00 ± 0.16	**1.21 ± 0.08**	*2.65*
Primary Visual Cortex	0.96 ± 0.10	1.02 ± 0.12	*0.54*	0.96 ± 0.07	*0.00*	1.02 ± 0.02	*0.83*	0.97 ± 0.03	**1.15 ± 0.14**	*1.56*
Gyrus Angularis	1.18 ± 0.13	1.29 ± 0.13	*0.85*	1.16 ± 0.09	*-0.18*	1.33 ± 0.05	*1.52*	1.24 ± 0.23	**1.36 ± 0.10**	*1.55*
Temporoccipital	1.23 ± 0.12	1.32 ± 0.12	*0.75*	1.18 ± 0.08	*-0.49*	1.38 ± 0.09	*1.41*	1.23 ± 0.22	1.36 ± 0.08	*1.27*
Lateral Temporal	1.23 ± 0.12	**1.35 ± 0.12**	*1.00*	1.22 ± 0.09	*-0.09*	1.28 ± 0.03	*0.57*	1.31 ± 0.21	1.34 ± 0.07	*1.12*
Inferior Temporal	1.10 ± 0.15	**1.26 ± 0.21**	*0.88*	1.08 ± 0.15	*-0.13*	0.94 ± 0.07	*-1.37*	1.27 ± 0.37	1.21 ± 0.20	*0.62*
Amygdala	1.75 ± 0.16	1.80 ± 0.14	*0.33*	1.81 ± 0.12	*0.42*	1.86 ± 0.09	*0.85*	1.98 ± 0.09	1.66 ± 0.23	*-0.45*
Hippocampus	1.60 ± 0.11	1.61 ± 0.12	*0.09*	1.62 ± 0.11	*0.18*	1.64 ± 0.06	*0.45*	1.58 ± 0.20	**1.44 ± 0.08**	*-1.66*
Parahippocampus	1.36 ± 0.16	1.38 ± 0.17	*0.12*	1.37 ± 0.12	*0.07*	1.16 ± 0.15	*-1.29*	1.17 ± 0.44	1.17 ± 0.20	*-1.05*
Entorhinal Cortex	0.87 ± 0.25	0.78 ± 0.17	*-0.42*	0.77 ± 0.24	*-0.41*	0.72 ± 0.20	*-0.66*	1.00 ± 0.16	0.84 ± 0.29	*-0.11*
Caudate	2.44 ± 0.26	2.40 ± 0.27	*-0.15*	2.37 ± 0.32	*-0.24*	2.11 ± 0.31	*-1.15*	2.48 ± 0.28	2.15 ± 0.15	*-1.37*
Putamen	2.16 ± 0.22	2.10 ± 0.09	*-0.36*	2.19 ± 0.19	*0.15*	2.13 ± 0.10	*-0.18*	2.01 ± 0.15	1.99 ± 0.12	*-0.96*
Globus Pallidus	1.85 ± 0.09	**1.74 ± 0.08**	*-1.29*	1.86 ± 0.11	*0.10*	1.78 ± 0.04	*-1.01*	1.81 ± 0.05	**1.69 ± 0.08**	*-1.88*
Thalamus	2.26 ± 0.20	2.28 ± 0.14	*0.12*	2.28 ± 0.20	*0.10*	2.19 ± 0.14	*-0.41*	2.27 ± 0.04	2.15 ± 0.20	*-0.55*
Midbrain	1.27 ± 0.14	1.33 ± 0.14	*0.43*	1.26 ± 0.06	*-0.09*	1.45 ± 0.07	*1.63*	1.31 ± 0.15	1.39 ± 0.11	*0.95*
Pons	1.44 ± 0.12	1.49 ± 0.12	*0.42*	1.48 ± 0.11	*0.35*	1.36 ± 0.02	*-0.93*	1.56 ± 0.09	1.33 ± 0.14	*-0.84*

Abbreviations

CN: elderly controls; MCI: mild cognitive impairment; AD: Alzheimer's disease; SUVR: Standard Uptake Value Ratio; WM: white matter (reference region)

In red bold: *Significantly higher than controls (p<0.05)*
In blue bold: *Significantly lower than controls (p<0.05)*
In green bold: *Cohen's effect size* d *against Aβ- CN*

SUPPLEMENTARY TABLE 3. Association between regional ^{18}F-SMBT-1 binding and brain volumetrics

	Hippocampus (n=73)		Grey Matter (n=73)		White Matter (n=73)		Ventricles (n=73)		White Matter Hyperintensities (n=72)	
SMBT-1 Region	**r**	***p***	**r**	***p***	**r**	***p***	**r**	***p***	**r**	***p***
Ventrolateral Prefrontal	-0.016	*0.893*	0.004	*0.975*	0.014	*0.905*	0.088	*0.459*	0.140	*0.241*
Orbitofrontal	0.033	*0.781*	0.010	*0.933*	0.083	*0.483*	0.077	*0.516*	0.056	*0.638*
Anterior Cingulate	0.212	*0.072*	0.104	*0.383*	-0.105	*0.379*	0.045	*0.703*	-0.041	*0.734*
Posterior Cingulate	-0.097	*0.413*	-0.187	*0.110*	0.084	*0.482*	0.146	*0.219*	0.098	*0.412*
Superior Parietal	-0.188	*0.112*	-0.192	*0.104*	0.134	*0.260*	0.198	*0.094*	0.206	*0.083*
Supramarginal Gyrus	-0.228	*0.052*	-0.280	*0.017**	0.069	*0.562*	0.093	*0.436*	0.134	*0.262*
Lateral Occipital	-0.282	*0.016**	-0.225	*0.055*	0.145	*0.220*	0.070	*0.559*	0.253	*0.032**
Primary Visual Cortex	-0.198	*0.093*	-0.180	*0.129*	0.011	*0.928*	0.035	*0.766*	0.279	*0.018**
Gyrus Angularis	-0.159	*0.180*	-0.170	*0.150*	0.149	*0.209*	0.045	*0.705*	0.151	*0.206*
Temporoccipital	-0.143	*0.228*	-0.084	*0.479*	0.166	*0.161*	0.011	*0.930*	0.042	*0.728*
Lat Temporal	-0.064	*0.588*	-0.021	*0.861*	0.210	*0.074*	0.007	*0.954*	-0.017	*0.885*
Inferior Temporal	-0.007	*0.957*	-0.042	*0.722*	0.323	*0.005**	-0.169	*0.153*	0.022	*0.855*
Amygdala	0.118	*0.322*	0.166	*0.160*	0.427	*0.000**	-0.073	*0.542*	0.037	*0.761*
Hippocampus	0.343	*0.003**	0.337	*0.004**	0.232	*0.048**	-0.071	*0.554*	-0.231	*0.051*
Parahippocampus	0.338	*0.004**	0.331	*0.004**	0.080	*0.499*	-0.274	*0.019**	-0.253	*0.032*
Entorhinal	0.031	*0.792*	0.034	*0.775*	0.052	*0.662*	-0.013	*0.911*	0.132	*0.268*
Caudate	0.201	*0.089*	0.303	*0.009**	-0.063	*0.594*	-0.198	*0.093*	-0.170	*0.155*
Putamen	-0.018	*0.883*	0.197	*0.129*	-0.194	*0.101*	0.060	*0.616*	-0.058	*0.630*
Globus Pallidus	0.115	*0.332*	0.321	*0.006**	0.130	*0.273*	-0.056	*0.636*	-0.056	*0.639*
Thalamus	0.235	*0.046**	0.303	*0.009**	0.062	*0.604*	-0.151	*0.203*	-0.074	*0.539*
Midbrain	0.069	*0.560*	0.163	*0.171*	0.347	*0.003**	0.002	*0.984*	-0.007	*0.951*
Pons	0.163	*0.169*	0.250	*0.033**	0.221	*0.060*	-0.050	*0.678*	-0.137	*0.252*
Aβ burden (CL)	-0.432	*0.000**	-0.449	*0.000**	-0.031	*0.793*	0.207	*0.078*	0.218	*0.065*
Tau burden (SUVR)	-0.358	*0.003**	-0.410	*0.001**	0.018	*0.886*	0.204	*0.093*	-0.184	*0.129*

**Significantly associated (p<0.05)*